Life Sciences 232 (2019) 116678

Contents lists available at ScienceDirect

Life Sciences

journal homepage: www.elsevier.com/locate/lifescie

Sclareol is a potent enhancer of doxorubicin: Evaluation of the free combination and co-loaded nanostructured lipid carriers against breast cancer

Gabriel Silva Marques Borges[a], Juliana de Oliveira Silva[a], Renata Salgado Fernandes[a], Ângelo Malachias de Souza[b], Geovanni Dantas Cassali[c], Maria Irene Yoshida[d], Elaine Amaral Leite[a], André Luis Branco de Barros[e], Lucas Antônio Miranda Ferreira[a,*]

[a] Department of Pharmaceutics, Faculty of Pharmacy, Federal University of Minas Gerais, Belo Horizonte, Minas Gerais, Brazil
[b] Department of Physics, Exact Sciences Institute, Federal University of Minas Gerais, Belo Horizonte, Minas Gerais, Brazil
[c] Department of General Pathology, Biologic Sciences Institute, Federal University of Minas Gerais, Belo Horizonte, Minas Gerais, Brazil
[d] Department of Chemistry, Exact Sciences Institute, Federal University of Minas Gerais, Belo Horizonte, Minas Gerais, Brazil
[e] Department of Clinical Analyses and Toxicology, Faculty of Pharmacy, Federal University of Minas Gerais, Belo Horizonte, Minas Gerais, Brazil

ARTICLE INFO

Keywords:
Doxorubicin
Sclareol
Co-encapsulation
Synergism
Breast cancer
Nanostructured lipid carriers

ABSTRACT

Aims: In this work, it was sought to determine if there was synergism between doxorubicin (DOX), a well-known antineoplastic, and sclareol (SC), a diterpene from natural origin, in breast cancer treatment. Moreover, it was investigated if their co-loading in the same nanocarrier would result in a gain of activity and/or a toxicity diminishment.

Main methods: The synergism of the DOX:SC combination was evaluated in MDA-MB-231 and 4T1 cells. A nanostructured lipid carrier (NLC) co-encapsulating DOX and SC in their synergistic molar ratio was prepared and characterised, in terms of mean diameter, zeta potential, DOX encapsulation efficiency, small angle X-ray scattering, differential scanning calorimetry, and polarised light microscopy for further intravenous administration. The anticancer activity of the combination, free and encapsulated, was evaluated in 4T1-tumour bearing mice.

Key findings: It was determined that DOX:SC combination at the molar ratio 1:1.9 presents better synergistic anticancer activity than the molar ratio 1:7.5 *in vitro*. DOX:SC-loaded NLC (NLC-DOX-SC) improved *in vitro* cytotoxic and *in vivo* antitumour activity compared to free DOX. Although NLC-DOX-SC and free DOX:SC, at the synergistic molar ratio, showed similar activity in the *in vivo* study, the free combination provoked body weight loss, behaviour alterations and haematological toxicity in the animals, while this was not observed for NLC-DOX-SC.

Significance: This work shows that SC and DOX present synergistic anticancer activity for breast cancer treatment whereas NLC-DOX-SC was a feasible alternative to attain the benefits posed by DOX:SC combination but with none to fewer side effects.

1. Introduction

Doxorubicin (DOX) (Fig. 1A) is an anthracycline drug that can be used in most of the cancer types, including several types of solid tumours [1,2]. Although very effective, the chronic clinical use of DOX is limited due to its severe toxicity, leading to serious complications, including patients' death [1,3]. In that way, the combination of multiple drugs might result in higher antitumor activity, leading to a reduction of side effects since lower concentrations of each drug is needed to get the desired effect [4].

Sclareol (SC) (Fig. 1B) is a labdane diterpene from natural origin that has shown important anticancer activity [5–11]. When evaluated together *in vitro*, DOX and SC produced higher cytotoxic and cytostatic effects [12,13]. Nevertheless, this combination has never been administered *in vivo* before. Despite the possible benefits of DOX and SC *in vivo* co-administration, some problems may arise: firstly, SC is a very

* Corresponding author at: Department of Pharmaceutics, Faculty of Pharmacy, Universidade Federal de Minas Gerais (UFMG), Avenida Antônio Carlos, 6627, Campus Pampulha, CEP 31270-901 Belo Horizonte, Minas Gerais, Brazil.
E-mail address: lucas@farmacia.ufmg.br (L.A.M. Ferreira).

https://doi.org/10.1016/j.lfs.2019.116678
Received 7 February 2019; Received in revised form 14 July 2019; Accepted 20 July 2019
Available online 22 July 2019

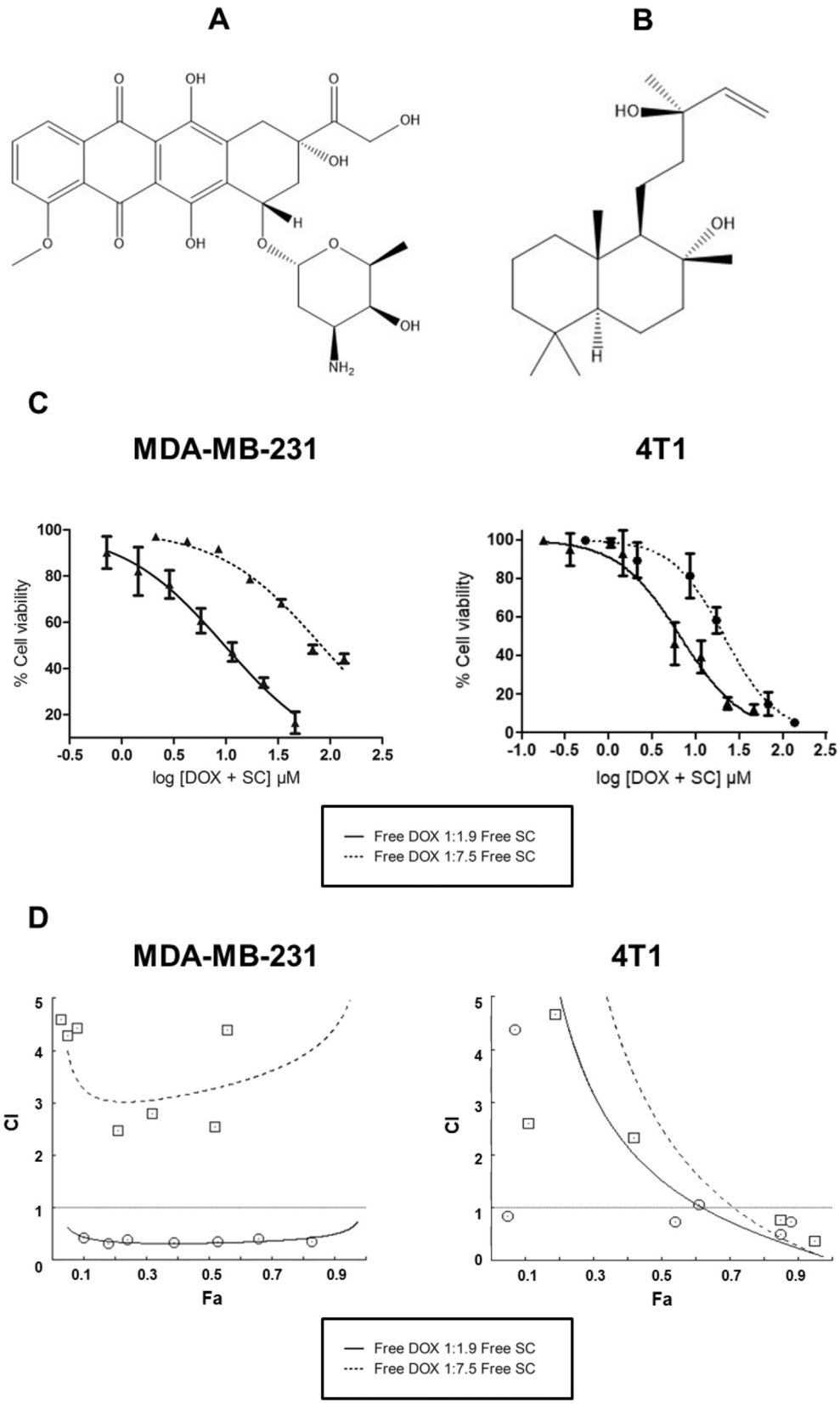

Fig. 1. Chemical structure of (A) DOX and (B) SC. (C) Cell viability and (D) CI × Fa curves for DOX:SC combinations (1:1.9 and 1:7.5 molar ratios) for MDA-MB-231 and 4T1 cells after incubation for 24 h. Values are expressed as mean ± standard deviation, n = 3.
Abbreviation: SC, sclareol; DOX, doxorubicin; CI, combination index; Fa, fraction affected; MDA-MB-231, human breast adenocarcinoma cell line; 4T1; murine breast cancer cell line.

hydrophobic drug (log P around 5) and it is difficult to deliver enough amounts of it by intravenous route [8]; secondly, as different molecules can have different pharmacokinetics, if SC and DOX arrive in the tumour site in different moments, their synergism can be lost [13].

DOX and SC nanoencapsulation could solve both issues as it could allow SC administration and the simultaneous arrival of DOX and SC in the tumour site through coordinated pharmacokinetics [14]. Interesting choices of nanocarriers are nanostructured lipid carriers (NLC). NLC are nanocarriers that have emerged in the last decade, being increasingly used due to their advantages as high stability, low toxicity and high drug loading [15]. Nevertheless, it is known that not all the ratios used between two drugs lead to synergistic effects [4]. Consequently, it is of great importance to determine which DOX:SC molar ratio presents synergistic activity in order to be loaded in the NLC.

Therefore, this work has proposed to evaluate the synergism between DOX and SC against two triple negative breast cancer models: *in vitro*, in the human breast cancer cell line (MDA-MB-231) and both *in vitro* and *in vivo* in the murine breast cancer cell line, 4T1, in their free form and co-loaded in NLC.

2. Materials and methods

2.1. Materials

DOX hydrochloride was purchased from ACIC Chemicals (Ontario, Canada). Tetrahydrofuran (THF) and Methanol (MeOH) were purchased from Tedia (Fairfield, USA). Triethanolamine was purchased from Merck (Darmstadt, Germany). Compritol® 888 ATO (a mixture of mono-, di-, and tri-glycerides of behenic acid) was kindly provided by Gattefossé (Saint-Priest, France). Ethoxylated sorbitan monoleate (Tween™ 80) and peanut oil were kindly provided by Croda (Pennsylvania, USA). Polyethylene glycol 400, oleic acid and SC were obtained from Sigma-Aldrich (St. Louis, USA). Ethanol 96% was obtained from Synth (São Paulo, Brazil). Cell Titer Blue® (CTB) was obtained from Promega (Madison, USA). Dulbecco's Modified Eagle's Medium (DMEM), Fetal Bovine Serum (FBS) and penicillin were purchased from Gibco Life Technologies (Waltham, USA). Other substances used were of analytical grade without further purification.

2.2. Preparation of NLC

NLC loading both DOX and SC (NLC-DOX-SC), loading only DOX (NLC-DOX), and Blank-NLC (without DOX and without SC) were produced. The composition of the oily phase (OP) and aqueous phase (AP) of the nanocarriers is described in Table 1 [16]. First, the OP was heated to 80 °C while the AP was also heated separately to the same temperature. With the temperature maintained at 80 °C, AP was gently dropped onto the OP under constant agitation, at 8000 rpm, with an Ultra Turrax T-25 homogeniser (Ika Labortechnik, Staufen, Germany).

Table 1
Composition (% w/v) of Blank-NLC, NLC-DOX, and NLC-DOX-SC.

		Blank-NLC	NLC-DOX	NLC-DOX-SC
OP	Compritol® 888 ATO	1.20	1.20	1.20
	Peanut oil	0.30	0.30	0.30
	Tween™ 80	0.80	0.80	0.80
	Triethanolamine	0.06	0.06	0.06
	Oleic acid	0.10	0.10	0.10
	DOX	—	0.05	0.05
	SC	—	—	0.05
AP	Water	100	100	100

Abbreviations: DOX, doxorubicin; SC, sclareol; Blank-NLC, unloaded nanostructured lipid carrier; NLC-DOX, doxorubicin loaded nanostructured lipid carrier; NLC-DOX-SC, doxorubicin and sclareol in their synergic molar ratio co-loaded nanostructured lipid carrier.

The formed emulsion was immediately submitted to a high-intensity probe sonication for 10 min. After this period, the formulations were cooled down to room temperature with manual agitation. The pH was adjusted to 7.0–7.5 with a solution of 0.1 M HCl and the formulations were stored at 4 °C, protected from light in a nitrogen atmosphere.

2.3. Cell culture

ATCC® HTB-26 (MDA-MB-231), a human breast adenocarcinoma cell line, and ATCC® CRL-2539 (4T1), a murine breast cancer cell line, were purchased from ATCC® (American Type Culture Collection, Manassas, USA). Cells were grown and maintained in DMEM medium supplemented with FBS (10% v/v) and penicillin (100 IU/mL) in a 5% CO_2 atmosphere at 37 °C.

2.4. Cytotoxicity assay and synergism analysis

Cell viability was measured with CTB cell viability assay. Cells were seeded in 96-well tissue culture plates at a cell concentration of 5×10^3 cells/well about 24 h before the treatment. NLC and free DOX solutions were freshly prepared by diluting them in ultrapure water. Free SC solutions were prepared through SC solubilisation in DMSO. The cells were incubated with free DOX and SC solutions alone or in combination (molar ratio of DOX:SC, 1:1.9 and 1:7.5) and with the NLC for 24 h, washed thrice with complete DMEM, and then supplemented with 40 µL of DMEM and 10 µL of CTB reagent. The incubation was performed for 2 h and the fluorescence intensity was measured using a Cytation™ 5 equipment (BioTek, Winooski, USA) at 530/590 nm excitation/emission wavelengths. Solvent control (DMSO) was done. All experiments were performed in triplicate and IC_{50} values were calculated with GraphPad Prism® 5 software.

Synergism or antagonism between free DOX and SC was calculated with CompuSyn® software by analysing CI (combination index) *versus* Fa (fraction affected). CI values lower than 1 indicate synergism, higher than 1 indicate antagonism, and close to 1 refer to an additive effect. Fa represents the percentage of cell death with 0 being a state where no death was detected and 1 as a state of 100% of cell death [4].

2.5. NLC characterisation

2.5.1. Measurement of particle size and zeta potential

The mean particle diameter and zeta potential (ZP) of the NLC were measured by Dynamic Light Scattering (DLS) and DLS coupled with electrophoretic mobility, respectively, using Zetasizer Nano-ZS90 (Malvern Instruments, Malvern, United Kingdom) with a fixed angle (90°) laser beam at 25 °C. The formulations were diluted in ultrapure water 100 times before the analyses. All experiments were performed in triplicate. The data were reported as average size, polydispersity index (PdI) and ZP.

2.5.2. Differential scanning calorimetry (DSC)

Blank-NLC, NLC-DOX, and NLC-DOX-SC were analysed in their lyophilised form. The lyophilisation of the nanocarriers was performed using a freeze-dryer (Modulyo Freeze Dryer, Thermo Fisher, USA) connected to a VLP120 vacuum pump (ThermoFisher, Waltham, USA). The nanocarriers were rapidly frozen with the aid of liquid nitrogen and lyophilised at a temperature of −45 °C for 24 h.

Bulk materials (Compritol® 888 ATO, DOX, and SC) and lyophilised nanocarriers were placed in aluminum pans. DSC analyses were performed in a DSC-60 differential scanning calorimeter (Shimadzu, Kyoto, Japan). The heating rate was 10 °C/min with a nitrogen flow of 50 mL/min. The temperature range was 45–300 °C.

The results were expressed in: PT (melting peak temperature), OT (melting onset temperature), ET (melting endset temperature), and ΔT (difference between melting onset and endset temperatures).

2.5.3. Small-angle X-ray scattering (SAXS)

SAXS measurements were carried out at the SAXS1 beamline of the Brazilian Synchrotron Light Laboratory (LNLS, Campinas, Brazil), using a fixed X-ray wavelength ($\lambda = 0.1488$ nm). The scattered X-ray photons were detected using a Pilatus 300 K detector, covering a momentum transfer reciprocal space range of $0.5 < Q < 4.5\,nm^{-1}$; where $Q = (4\pi/\lambda)\,sin\theta$, and θ is the scattering angle.

The lyophilised samples and Compritol® 888 ATO were placed inside metal rings that were sealed by a polyimide film (Kapton®). The lattice spacing was calculated from SAXS results using the formula $d = 2\pi/Q$, valid for the first-order peaks of all structure types analysed herein. Domain sizes (L) were extracted using the reciprocal space width (ΔQ) of the first order peak of each measurement, as $L = 2\pi/\Delta Q$. An intrinsic instrument broadening of $0.01\,nm^{-1}$ was considered for all calculations.

2.5.4. Polarised light microscopy (PLM)

The full encapsulation of SC within NLC-DOX-SC was evaluated by an optical microscope (ZeissAxio Imager.M2, Carl Zeiss, Oberkochen, Germany) coupled with a light polariser and equipped with an AxioCam digital camera (Model ERc 5S, Carl Zeiss, Oberkochen, Germany). The samples were prepared in microscope slides (undiluted) and the detection of SC crystals by PLM would indicate precipitation of SC, showing that it was not successfully loaded within NLC-DOX-SC. As a control, a dispersion of SC in ultrapure water was prepared with the same SC concentration of NLC-DOX-SC, *i.e.*, 0.5 mg/mL, and also analysed by PLM, in the same way.

2.5.5. DOX encapsulation efficiency (DOX EE)

The DOX EE in NLC-DOX and NLC-DOX-SC was determined by the ultrafiltration method using centrifugal devices (Amicon®Ultra4 100 kDa, Millipore, Burlington, USA). DOX concentration in the nanocarriers was determined by HPLC with fluorimetric detention as previously described [17]. Briefly, the stationary phase was a reverse phase column (C_8, 250 mm × 4.6 mm × 5 μm) and the mobile phase consisted in a mixture of phosphate buffer 0.01 mol/L pH 3.0:MeOH (35:65). The flow rate was 1 mL/min and the injection volume was 20 μL. Excitation and emission wavelengths were 470 and 555 nm, respectively.

To evaluate the total concentration of DOX, aliquots of NLC-DOX and NLC-DOX-SC suspensions were dissolved first in THF, then in MeOH, and later in the mobile phase, before injection in HPLC.

To evaluate the non-encapsulated (water soluble) DOX, an aliquot (2 mL) of each NLC was submitted to ultrafiltration (10 min at 2400 rpm). Next, the ultrafiltrate was solubilised in MeOH, then in the mobile phase, and quantified in HPLC. To eliminate the binding of DOX in the devices, a pre-treating of the filters was performed. The devices were soaked in a passivating solution (Tween™ 20, 5% w/v), maintained overnight at room temperature, and washed with distilled water prior to use.

The DOX EE was calculated using the following equation: $EE\,\% = (CT - CAP)/CT \times 100$. Where: CT = total DOX concentration in each NLC and CAP = DOX concentration in the aqueous phase (non-encapsulated) of each NLC. Therefore, we consider that all DOX not present in the aqueous phase was successfully loaded in the NLC.

2.5.6. In vitro release of DOX from NLC-DOX-SC

In vitro DOX release study from NLC-DOX-SC was performed using the dialysis method. The external medium was phosphate-buffered saline (PBS) pH 7.4. Cellulose ester membrane dialysis tubes (cutoff size of 14,000 Da; diameter of 21 mm) (Sigma-Aldrich, St. Louis, USA) were filled with 2 mL of NLC-DOX-SC, sealed, and incubated with 50 mL of external medium, for 24 h at 37 °C, under magnetic stirring. An aqueous solution of DOX (0.5 mg/mL) was used as a control (free DOX). At various time points, aliquots were withdrawn and DOX concentration was quantified. The values were plotted as a cumulative percentage of DOX release. Released DOX (%) = RF/CD × 100. Where: RF = released fraction of DOX to the external medium and CD = initial concentration of DOX inside the dialysis bag.

2.6. In vivo study

2.6.1. Antitumour activity

Female BALB/c mice (5 weeks old, around 20 g, n = 6) received, subcutaneously, into the right thigh, aliquots (100 μL) of 4T1 (2.5×10^6) tumour cells. After 8 days of the inoculation, the mice were randomly assigned into five groups: Blank-NLC, free DOX, NLC-DOX, free DOX + free SC (DOX:SC in the synergistic molar ratio of 1:1.9), and NLC-DOX-SC. For all treatments, DOX and SC doses were 4 mg/kg/day, in a total of 5 administrations, every 3 days, injected by the tail vein. Hence, the total doses of DOX and SC in the treatment groups were 20 mg/kg. Free DOX was solubilised in ultrapure water and SC was solubilised in a mixture of ultrapure water (80% v/v), ethanol 96% (10% v/v), polyethylene glycol 400 (5% v/v), and Tween™ 80 (5% v/v), as already similarly reported [7]. Blank-NLC, NLC-DOX, and NLC-DOX-SC were administrated without prior dilution. Throughout the study, the behaviour of the animals was observed in order to evaluate the possible side effects of the treatments.

Tumours were measured with a calliper and mice were weighted every 2 days, starting 4 days after the first treatment administration. Absolute tumour volumes were calculated from the formula: $V = (d1)\,2 \times d2 \times 0.5$, where d1 and d2 represent the smaller and larger diameters, respectively. Relative tumour volumes were calculated from the formula: $V_x/V_0 \times 100$, being V_x the tumour volume in a specific day and V_0 being the tumour volume in the first day of treatment administration. Tumour doubling time was calculated from the formula: $t \times \ln 2/\ln (V_f/V_0)$, being t the period in days from the first to the last day of treatment, V_f being the absolute volume of the tumour in the last day of treatment and V_0 being the tumour volume in the first day of treatment administration.

After euthanasia, the tumours of the animals were weighted and the final tumour weight was calculated. All the experimental procedures were approved by the ethical committee for animal experimentation of Federal University of Minas Gerais (CEUA) under the protocol 03/2018.

2.6.2. Haematological analyses

At the end of the treatment regimen, the animals were anesthetized with a mixture of ketamine (80 mg/kg) and xylazine (15 mg/kg) and blood was collected by puncture of the brachial plexus in tubes containing anticoagulant (ethylenediaminetetraacetic acid). Haematological parameters such as haemoglobin (HGB), number of red blood cells (RBC), total white blood cells (WBC), haematocrit (HCT), red cell distribution width (RDW), and platelets (PLT) were measured using automatic Hemovet 2330 equipment from Brasmed® (Paulínia, Brazil).

2.6.3. Biochemical analyses

After haematological analyses, blood was centrifuged at 5000 rpm during 10 min and plasma was obtained. Plasma was used to perform biochemical analyses such as urea, creatinine, AST (aspartate aminotransferase), and CK (creatine kinase). The biochemical tests were performed using commercial kits from Labtest® (Lagoa Santa, Brazil) through Bioplus BIO-2000 semiautomatic analyser equipment (São Paulo, Brazil).

2.6.4. Histopathological analyses

After euthanasia, tumour, kidneys, spleen, and heart were collected for histopathological analysis. Samples were fixed in buffered formalin 10%, dehydrated in alcohol and included in paraffin blocks. Longitudinal sections of 4 μm were obtained and stained with haematoxylin and eosin. The slides were evaluated by trained pathologists and images were captured by a camera connected to the optical

microscopes: Olympus BX-40 (Olympus, Tokyo, Japan) and Nikon SMZ-745 T (Nikon, Tokyo, Japan). Necrotic tumour relative area was quantified through the software ImageJ.

2.7. Data analysis

Statistical analyses were carried out using one-way analysis of variance (ANOVA) followed by Tukey's post-test (for IC_{50}, average size, PdI, ZP, DOX EE, tumour doubling time, tumour weight, haematological, and biochemical analyses). For cytotoxicity assays, DOX *in vitro* release, antitumour activity, and body weight, two-way ANOVA followed by Bonferroni's post-test was used. For all analyses, the difference was considered statistically significant when P value was lower than 0.05.

3. Results

3.1. In vitro synergism between DOX and SC

Fig. 1C shows cell viability curves for the two molar combinations between DOX and SC tested in MDA-MB-231 and 4T1 cells. It is possible to see that a higher cytotoxicity is found for the 1:1.9 (DOX:SC) molar ratio when compared to the 1:7.5 (DOX:SC) molar ratio for both cell lines, which is also shown by the IC_{50} values (Table 2). Synergism or antagonism of these combinations were also evaluated by CI × Fa represented in Fig. 1D. In the whole range of Fa, CI values were lower than 1 for 1:1.9 (DOX:SC) molar ratio and higher than 1 for 1:7.5 (DOX:SC) molar ratio for the MDA-MB-231 cells. For 4T1 cell line, in high Fa values, the 1:1.9 (DOX:SC) molar ratio is more synergic than the 1:7.5 (DOX:SC) molar ratio. Therefore, the molar ratio 1:1.9 (DOX:SC) was chosen to be co-loaded in NLC.

3.2. NLC characterisation

The results for average diameter, PdI, ZP, and DOX EE for all the formulations tested are shown in Table 3. No statistical differences were seen for the three nanocarriers regarding these parameters. DOX EE in NLC was high (~97%), while average diameter was low (~100 nm).

The different NLC were analysed by DSC (Fig. 2A) and SAXS (Fig. 2B) in order to understand the structuration of their lipid matrixes. All the NLC showed less defined peaks (higher ΔT) and lower melting temperature values (lower OT and PT) (Table 4) than Compritol® 888 ATO (the solid lipid of NLC matrix), in DSC (Fig. 2A). Therefore, the NLC are less crystalline than Compritol® 888 ATO. This can also be observed by the more intense peaks in SAXS for Compritol® 888 ATO when compared to the ones from the different NLC (Fig. 2B).

When ΔT is analysed by DSC (Table 4) and the domain sizes by SAXS (Fig. 2B), it is possible to see that these values are inversely correlated. This shows that DOX input within the NLC decreases their crystallinity, while SC input slightly increases the crystallinity of NLC. By analysing Table 4, it is possible to see that SC is very crystalline (low ΔT value), the opposite of DOX (high ΔT value). This is a possible explanation for their influence on NLC crystallinity.

Regarding the supramolecular organisation of the NLC, Compritol® 888 ATO shows three peaks in the positions $Q = 1.00\,nm^{-1}$, $2.01\,nm^{-1}$, and $3.01\,nm^{-1}$ (Fig. 2B). SAXS data for Blank-NLC, NLC-DOX, and NLC-DOX-SC exhibit similar peak sequences of $Q = 1.07\,nm^{-1}$, $2.14\,nm^{-1}$, and $3.23\,nm^{-1}$. All these peaks follow approximately the same Q ratio of 1:2:3, indicating a lamellar packing with abrupt interfaces, leading to a well-defined electron density profile (the Fourier transform of a square wave profile has stronger peaks at odd orders). The shift to higher Q values of the peaks from the NLC is related to their smaller lattice spacing (Blank-NLC = 5.86 nm, NLC-DOX = 5.96 nm, and NLC-DOX-SC = 5.86 nm) compared to Compritol® 888 ATO (6.26 nm). Regarding the domain size (L), it is a parameter that is correlated with the inverse of the reciprocal space width (ΔQ) of the peaks ($L = 2\pi/\Delta Q$). For this parameter, we can also see that Compritol® 888 ATO has the larger L value (L = 81 nm) if compared to the NLC: Blank-NLC (L = 71 nm), NLC-DOX (L = 49 nm), and NLC-DOX-SC (L = 53 nm).

The comparison between the NLC also allows us to know how DOX and SC are interacting with the lipid matrix, providing indications if their encapsulation was successful. Analysing the DSC curves for Blank-NLC, NLC-DOX, and NLC-DOX-SC (Fig. 2A), it can be seen that their melting temperature values (OT and PT) are very similar (Table 4). This is a strong indicator that DOX and SC were fully encapsulated in the NLC, not destabilising the lipid matrix. Moreover, as DLS (Table 3), DSC (Fig. 2A), and SAXS (Fig. 2B) analyses showed very similar results for NLC-DOX and NLC-DOX-SC, this is a strong evidence of good SC encapsulation.

In order to deeply investigate whether the encapsulation of SC in NLC-DOX-SC was effective, this formulation was analysed by PLM, as well as a dispersion of SC in ultrapure water (the dispersive medium of NLC-DOX-SC) (Fig. 2C). The presence of SC crystals was clearly visualised in the SC dispersion when it was submitted to polarised light. This was expected as SC is a very hydrophobic molecule. Nevertheless, SC crystals were not visualised for NLC-DOX-SC, proving that a good encapsulation of SC was obtained.

Finally, DOX release was significantly lower for NLC-DOX-SC in all the times evaluated (Fig. 3A). In 24 h, DOX released fraction from free DOX was close to 80% (78.0 ± 4.2%), while DOX release from NLC-DOX-SC was much lower: 24.2 ± 5.1%. Therefore, NLC-DOX-SC showed to control DOX release *in vitro* (Fig. 3A).

Table 2
IC_{50} values of free DOX and free SC alone and in combination (in DOX:SC 1:1.9 and 1.7.5 molar ratios) in MDA-MB-231 and 4T1 cell lines, after 24 h of incubation. Values are expressed as mean ± standard deviation, n = 3.

IC_{50} (μM)	MDA-MB-231	4T1
Free DOX	33.9 ± 7.7[c]	3.8 ± 1.5[b,c]
Free SC	27.6 ± 2.1[c]	38.2 ± 9.3
Free DOX 1:1.9 free SC	9.6 ± 1.3[a,b,c]	6.6 ± 1.2[b,c]
Free DOX 1:7.5 free SC	82.5 ± 6.3	21.2 ± 5.8

Abbreviations: DOX, doxorubicin; SC, sclareol; MDA-MB-231, human breast adenocarcinoma cancer cell line; 4T1, murine breast cancer cell line; IC_{50}, concentration that kills 50% of the cells under treatment.
Statistics: One-way analysis of variance (ANOVA) followed by Tukey's *t*-test, $P < 0.05$.
[a] Statistically different from free DOX.
[b] Statistically different from free SC.
[c] Statistically different from free DOX 1:7.5 free SC.

Table 3
Average size, PdI, ZP, and DOX EE of Blank-NLC, NLC-DOX, and NLC-DOX-SC. Values are expressed as mean ± standard deviation, n = 3.

	Average size (nm)	PdI	ZP (mV)	DOX EE (%)
Blank-NLC	113 ± 12	0.30 ± 0.04	−28 ± 2	___
NLC-DOX	108 ± 7	0.21 ± 0.02	−30 ± 4	98 ± 1
NLC-DOX-SC	104 ± 12	0.23 ± 0.02	−31 ± 2	97 ± 2

Abbreviations: PdI, polydispersity index; ZP, zeta potential; EE, encapsulation efficiency; Blank-NLC, unloaded nanostructured lipid carrier, NLC-DOX, doxorubicin loaded nanostructured lipid carrier; NLC-DOX-SC, doxorubicin and sclareol in their synergic molar ratio co-loaded nanostructured lipid carrier.
Statistics: One-way analysis of variance (ANOVA) followed by Tukey's *t*-test (for average size, PdI, and ZP) and Student's *t*-test (for DOX EE), $P < 0.05$. Any difference was found regarding average size, PdI, ZP, and DOX EE for all the groups.

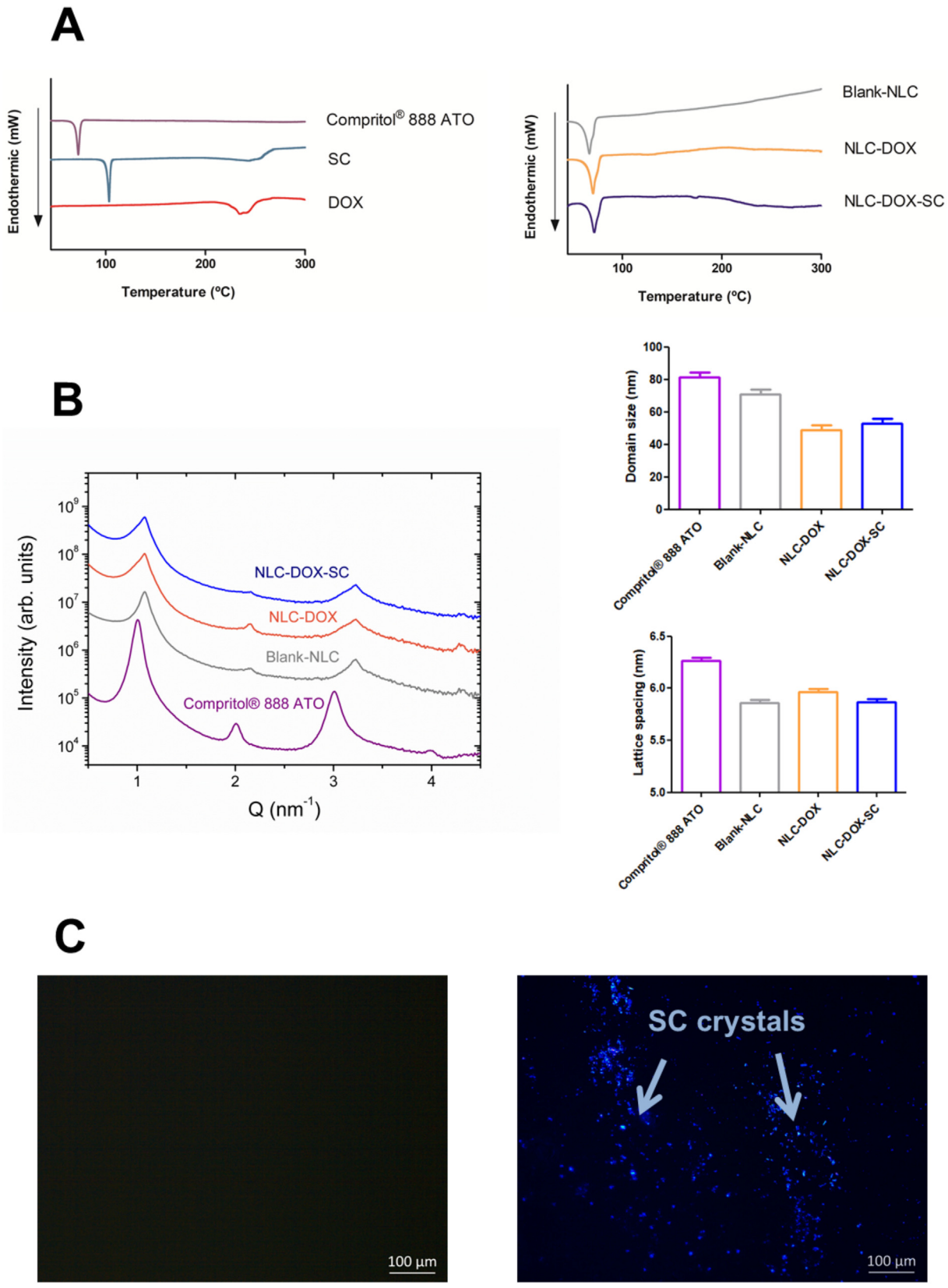

Fig. 2. (A) DSC curves of bulk materials and NLC; the temperature range used was 45–300 °C; (B) SAXS diffractograms of Compritol® 888 ATO and NLC with their lattice spacing and domain size; (C) PLM of NLC-DOX-SC (absence of SC crystals) and SC dispersion in ultrapure water (significant presence of SC crystals). Abbreviation: DSC, differential scanning calorimetry; NLC, nanostructured lipid carriers; SC, sclareol; DOX, doxorubicin; Blank-NLC, unloaded nanostructured lipid carriers; NLC-DOX, doxorubicin-loaded nanostructured lipid carriers; NLC-DOX-SC, doxorubicin and sclareol in their synergic molar ratio co-loaded nanostructured lipid carrier; SAXS, small-angle X-ray scattering; PLM, polarised light microscopy.

Table 4
Melting temperatures values for the NLC samples obtained by DSC. The temperature range used was 45–300 °C.

	OT (°C)	PT (°C)	ET (°C)	ΔT (°C)
Compritol® 888 ATO	69.64	72.45	74.58	4.94
SC	98.62	100.94	102.66	4.04
DOX	227.13	232.60	249.16	22.03
Blank-NLC	63.72	68.51	73.02	9.30
NLC-DOX	63.85	68.34	73.71	9.86
NLC-DOX-SC	64.58	69.11	73.97	9.39

Abbreviations: SC, sclareol; DOX, doxorubicin; NLC, nanostructured lipid carriers; Blank-NLC, unloaded nanostructured lipid carrier; NLC-DOX, doxorubicin loaded nanostructured lipid carrier; NLC-DOX-SC, doxorubicin and sclareol in their synergic molar ratio co-loaded nanostructured lipid carrier; DSC, differential scanning calorimetry; OT, onset melting temperature; PT, melting peak temperature; ET, endset melting temperature; ΔT, difference between the onset and endset melting temperatures.

3.3. NLC in vitro anticancer activity

It was seen that DOX:SC combination was synergistic in the 1:1.9 molar ratio in all the Fa range for MDA-MB-231 and in high Fa values for 4T1 cells. Therefore, it was sought to know if NLC-DOX-SC would enhance the anticancer activity of free DOX in these cell lines. NLC-DOX-SC and free DOX + free SC (DOX:SC molar ratio 1:1.9) show higher cytotoxic than free SC, free DOX, and NLC-DOX, in MDA-MB-231 and 4T1 cells (Fig. 3B). Blank-NLC as well as NLC-SC were also tested but did not show any diminishment of cell viability in all the concentrations tested. Cytotoxicity of NLC-DOX-SC and free DOX + free SC (in the synergistic molar ratio of DOX:SC 1:1.9) were very similar in both cell lines, showing that the synergism between DOX and SC is also seen when both molecules are co-loaded in NLC.

3.4. In vivo anticancer activity

As NLC-DOX-SC and free DOX + free SC (in the synergistic molar ratio of DOX:SC 1:1.9) showed an enormous potential to provide great *in vitro* anticancer activity (Fig. 3B), the formulations were tested *in vivo*, in a murine breast cancer model (4T1 tumour-bearing mice). Fig. 4A, B and Table 5 show that NLC-DOX-SC and free DOX + free SC had a higher capacity to inhibit tumour growth than Blank-NLC. In the meanwhile, free DOX and NLC-DOX absolute and relative tumour volumes were not statistically different from Blank-NLC. This shows that DOX alone (free DOX or NLC-DOX) is not an effective treatment in the dose regimen tested. The results found for the final tumour weight (Fig. 4C) also show better results for the combination between DOX and SC when compared to groups that did not present SC. These results prove the potential of DOX and SC combination in breast cancer treatment as it was already seen in the *in vitro* studies (Fig. 3B).

Moreover, representative tumour sections from Fig. 5 also indicate smaller tumour sizes for free DOX + free SC and NLC-DOX-SC groups. Light areas representing necrosis in the tumours are clearly seen for all the groups, with no significant differences in the necrotic tumour area between them (Fig. S1).

3.5. Preliminary toxicity of the treatments

The body weight of the animals was evaluated throughout the study in order to determine the preliminary toxicity of the treatments (Fig. 4D). NLC-DOX-SC provoked a lower body weight loss compared to free DOX + free SC, suggesting the ability of the NLC to reduce DOX toxicity. Moreover, it is important to underscore that the animals of the group free DOX + free SC became very agitated during the injection of free SC. These animals were angrier and with marked piloerection compared to the animals from the other groups throughout the study.

The haematological experiments (Table 6) also gave us important data about the toxicity of the treatments. We can see that NLC-DOX-SC evoked a lower reduction of RBC, HCT, HGB, and RDW values than free DOX + free SC. This is an indicative that NLC-DOX-SC is less myelosuppressive than free DOX + free SC.

In histopathological analyses (Fig. 5), the kidneys structure was preserved for all the groups. Nevertheless, great impact was shown by all the treatments (free DOX, NLC-DOX, free DOX + free SC, and NLC-DOX-SC) on spleen and liver over no-treated (Blank-NLC) animals. The animals that received Blank-NLC had splenomegaly and inflammatory infiltrates in the portal spaces of the liver (Fig. 5). All the treatments reduced spleen size and liver inflammation.

No signals of renal and liver damage caused by the treatments were found in biochemical analyses (Table 7). Urea values were all similar and the lower creatinine levels for NLC-DOX-SC are not clinically relevant. Although non-tumour bearing mice were not evaluated in the biochemical tests, by comparing the values obtained for the treated animals to the Blank-NLC group, one can indicate that liver and renal functions were not impaired due to the treatments.

Regarding cardiac function, free DOX slightly increased CK values (Table 7). NLC-DOX, NLC-DOX-SC, and free DOX + free SC did not show any increasement of CK values, indicating that nanoencapulation and SC presence could diminish this side effect. Nevertheless, in histopathological analyses, cardiac tissue seems to be preserved for all the groups, without the visualisation of hypotrophic, degenerative or inflammatory changes besides any hyaline degeneration in the cardiomyocytes (Fig. 5).

4. Discussion

Although many advances have emerged in breast cancer treatment, as hormone and targeted therapies, chemotherapy remains a vital therapeutic option especially for cancers that do not present hormone (oestrogen or progesterone) or human epidermal growth factor receptor-type 2 (HER2) receptors. These breast cancer types (triple negative) are very aggressive, and chemotherapy, as DOX, is the main treatment [19–21]. Therefore, this work has aimed to evaluate the synergism between DOX and SC in the triple negative (no hormone or HER2 receptors) cells, MDA-MB-231 and 4T1 [22], in their synergic ratio both free and co-loaded in NLC.

In this work, we have chosen SC as a natural compound to enhance DOX activity, after exciting anticancer results shown by this diterpene [5–13]. Natural products derivatives are an interesting class of molecules that can enhance the activity of well-established oncologic drugs. Past studies have shown that curcumin [23], docosahexaenoic acid [17,24,25], vitamin E derivatives [17,26], among others, enormously enhanced the *in vitro* and *in vivo* anticancer activity of DOX in nanocarriers.

First, it was evaluated if free DOX and free SC exhibit synergistic activity in MDA-MB-231 and 4T1 cells. DOX and SC combination was already tested in other cancer cells [12,13], but not for these lineages. From our knowledge, this is the first work that calculates CI values for SC combination with any drug. The results showing that DOX:SC molar ratio combination of 1:1.9 is more synergistic that 1:7.5 is of major importance as they show that the combination between different molecules should stick to certain ratios in order to produce optimal results. This is not an exclusivity of DOX and SC combination. As an example, DOX and resveratrol (another molecule from natural origin) were combined against MDA-MB-231 cells, and depending on the ratio used, the combination was synergistic or antagonistic [27].

The next step was to co-load DOX and SC in their synergistic molar ratio (DOX:SC of 1:1.9) within NLC (NLC-DOX-SC). NLC-DOX-SC had the intention to provide a safer therapy, as nanoencapsulation can decrease DOX side effects [28] and prevent possible loss of the *in vivo* activity of free drug combinations due to different pharmacokinetics of the molecules [14]. Co-encapsulation of drugs in a single nanocarrier is

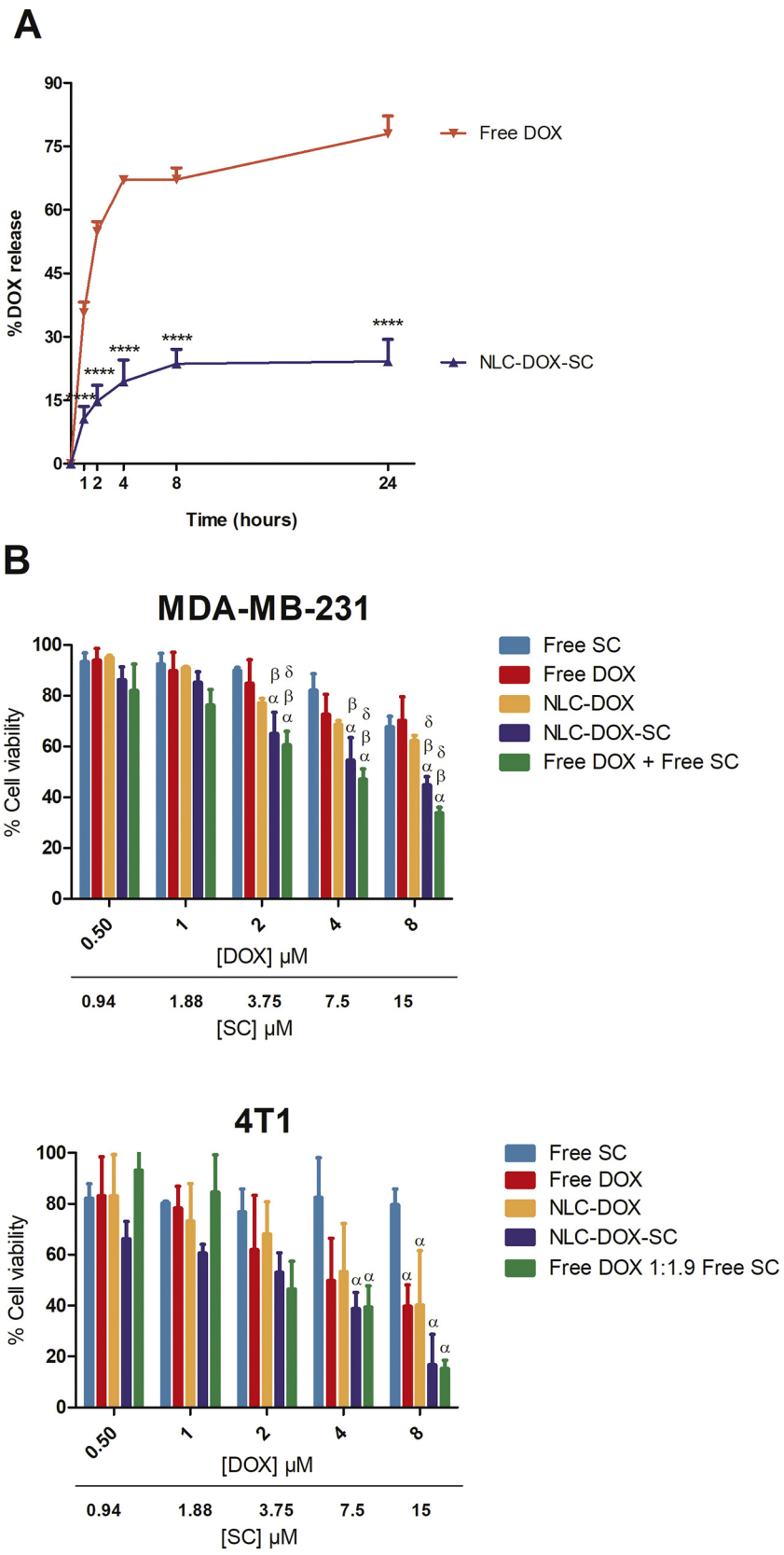

Fig. 3. (A) DOX accumulated release from free DOX aqueous solution and NLC-DOX-SC in PBS pH 7.40 medium. (B) Cell viability reduction caused by free DOX, free SC, free DOX + free SC, NLC-DOX, and NLC-DOX-SC in MDA-MB-231 and 4T1 cells after 24 h of incubation. Values are expressed as mean ± standard deviation, n = 3.
Note: **** = DOX release statistically different between free DOX and NLC-DOX-SC at that time point. $P < 0.0001$. α = cytotoxicity statistically different from free SC group ($P < 0.05$); β = cytotoxicity statistically different from free DOX group ($P < 0.05$); δ = cytotoxicity statistically different from NLC-DOX group ($P < 0.05$); Blank-NLC and NLC-SC were not represented as they did not cause cytotoxicity in the range of concentrations tested.
Abbreviation: DOX, doxorubicin; NLC-DOX-SC, doxorubicin and sclareol in their synergic molar ratio co-loaded nanostructured lipid carrier; PBS, phosphate buffer saline; SC, sclareol; NLC, nanostructured lipid carriers; MDA-MB-231, human breast adenocarcinoma cell line; 4T1, murine breast cancer cell line; Blank-NLC, unloaded nanostructured lipid carriers; NLC-DOX, doxorubicin-loaded nanostructured lipid carriers; free DOX + free SC, doxorubicin and sclareol in their synergic molar ratio.

a new trend in the nanomedicine research field, enhancing activity and reducing the toxicity of many antineoplastic drugs [29–32]. Recently, a liposome co-encapsulating cytarabine and daunorubicin (Vyxeos®) was approved by the FDA, after showing exciting results in patients with acute myeloid leukaemia in clinical trials [33].

NLC-DOX-SC had low average size and a narrow size distribution (PdI values below 0.30) indicating suitability for intravenous administration (Table 3). Particles with diameters lower than 200 nm can

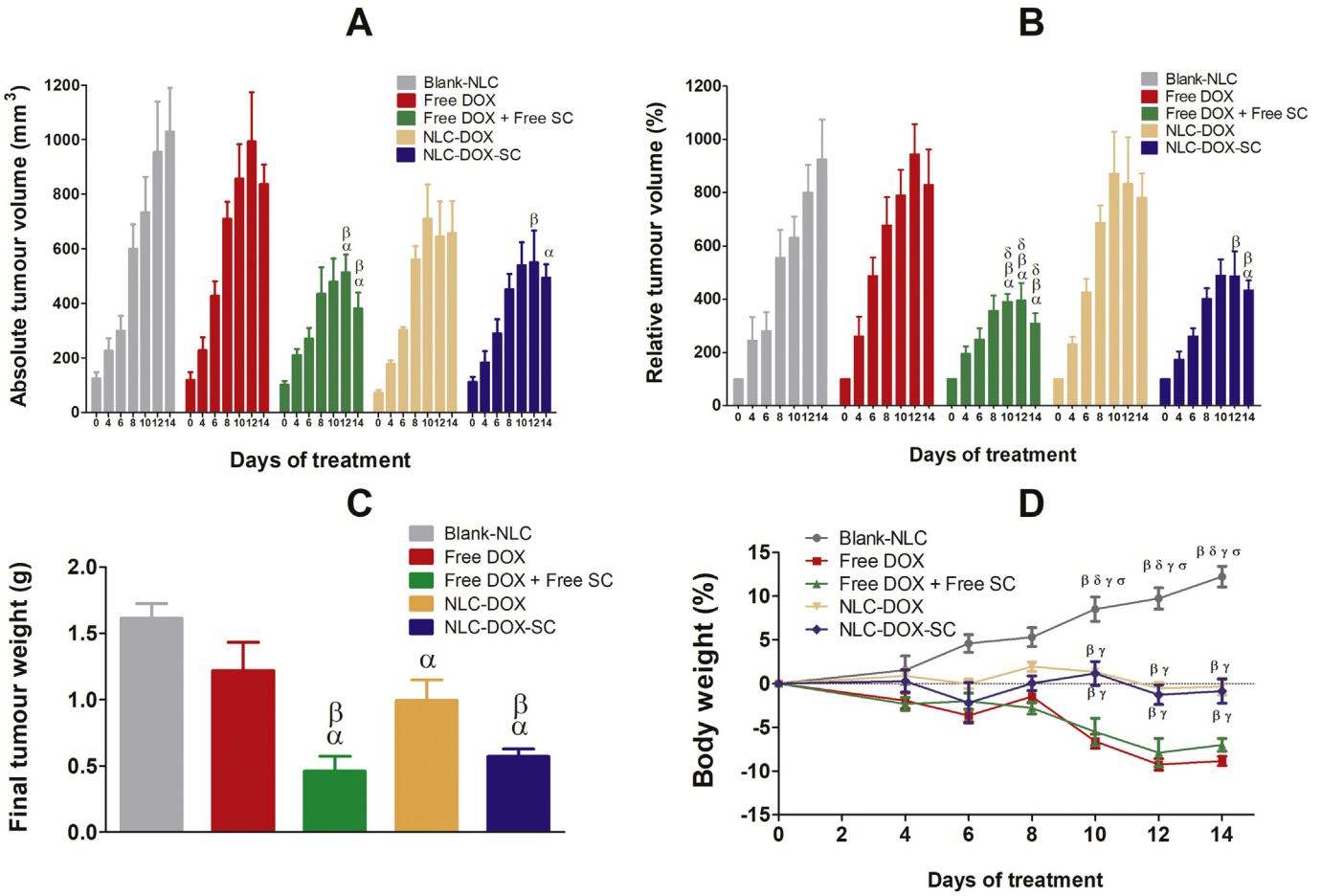

Fig. 4. (A) Absolute tumour volume throughout the treatments period (14 days); (B) Relative tumour volume throughout the treatments period (14 days); (C) Final tumour weight after 14 days of treatment; (D) Body weight variation throughout the treatments period (14 days). 5-weeks old female mice were inoculated with 4T1 cells subcutaneously and treatments were started after 8 days of inoculation. Values are expressed as mean ± standard error of the mean, n = 6.

Note: One-way ANOVA followed by Tukey's *t*-test (final tumour weight) and two-way ANOVA followed by Bonferroni's *t*-test (absolute and relative tumour volumes, and body weight variation) were used as statistic tests. α = statistically different from Blank-NLC ($P < 0.05$); β = statistically different from free DOX ($P < 0.05$); δ = statistically different from NLC-DOX ($P < 0.05$); γ = statistically different from free DOX + free SC ($P < 0.05$); σ = statistically different from NLC-DOX-SC ($P < 0.05$).

Abbreviation: 4T1, murine breast cancer cell line; DOX, doxorubicin; SC, sclareol;; Blank-NLC, unloaded nanostructured lipid carriers; NLC-DOX, doxorubicin-loaded nanostructured lipid carriers; NLC-DOX-SC, doxorubicin and sclareol in their synergic molar ratio co-loaded nanostructured lipid carrier; free DOX + free SC, doxorubicin and sclareol in their synergic molar ratio; ANOVA, analysis of variance.

accumulate in higher extension in tumour sites due to the EPR (enhanced permeation and retention) effect [34]. In that way, NLC-DOX-SC may be directed to tumours by a passive target mechanism, which might decrease DOX side effects.

The DOX EE within NLC was almost 100% (Table 3), which is in accordance with previous studies from our group [17,25–27,35]. This is due to the hydrophobic ion pair strategy. DOX presents an amino group in its glycosidic moiety that can form an ion pairing with the acid group of oleic acid, one of the constituents of the formulations. This ion pairing enhances the hydrophobicity of the conjugate, improving DOX encapsulation. This strategy has recently been reviewed by Oliveira et al. [36]. Regarding SC encapsulation in NLC-DOX-SC, efficient encapsulation was found by PLM (Fig. 2C).

The NLC were more deeply characterised by DSC and SAXS in order to understand the behaviour of the lipid matrix and its interactions with the loaded molecules, *i.e.* DOX and SC. It was shown that Compritol® 888 ATO is more crystalline than the NLC as already shown in other studies where the crystallinity of the nanocarriers was lower than the one of the bulk lipid [37,38]. Moreover, DOX input has decreased the crystallinity of the NLC and it was shown that NLC had a lamellar pattern of organisation, as previously reported for similar types of lipid nanocarriers [17,39,40].

Regarding the controlled release properties, NLC-DOX-SC could control DOX release (Fig. 3A). Several studies have shown a slower release of a drug when encapsulated in NLC [37,39] due to the fact that when a drug is nanoencapsulated, a mechanism is required to release it from the nanostructure: erosion, disintegration, or desorption [41], making this process slower than that seen for the solution of the free drug. This controlled release is important as it guarantees that DOX will be major released at tumour sites and not in systemic circulation leading to serious side effects. The rapid initial release of DOX followed by a plateau seen for NLC-DOX-SC is quite characteristic of drugs release from NLC [42]. This can be attributed to the fraction of the drug that is present on the outer surface of the NLC, whereas the plateau seen subsequently refers to the fraction present inside the NLC, which is more difficult to be released [41].

As appropriate physicochemical and DOX controlled release data were obtained, the NLC-DOX-SC potential to improve DOX anticancer activity was evaluated. NLC-DOX-SC showed similar activity from free DOX + free SC both *in vitro* (Fig. 3B) and *in vivo* (Fig. 4A, B, C and Table 5) in the 4T1 murine breast cancer model. Although 4T1 is not a human cell line, these cells produce an *in vivo* model that closely mimic

Table 5
Relative tumour volume (RTV), tumour growth inhibition ratio (IR), and tumour doubling time (DT) after 14 days of Blank-NLC, free DOX, NLC-DOX, free DOX + free SC, and NLC-DOX-SC administration in female 4T1 cells bearing Balb-c mice. Values are expressed as mean ± standard error of the mean, n = 6.

	RTV (%)	IR (%)	DT (days)
Blank-NLC	926 ± 149	—	4.6 ± 0.4
Free DOX	830 ± 133	10.4	5.0 ± 0.5
Free DOX + free SC	308 ± 39[a,b,c]	66.7	8.2 ± 1.2[a,b,c]
NLC-DOX	781 ± 92	15.7	4.7 ± 0.4
NLC-DOX-SC	433 ± 37[a,b]	53.2	6.6 ± 0.7

Abbreviations: RTV, Relative tumour volume; IR, tumour growth inhibition ratio; DT, tumour doubling time; Blank-NLC, unloaded nanostructured lipid carrier; NLC-DOX, doxorubicin loaded nanostructured lipid carrier; doxorubicin and sclareol in their synergic molar ratio co-loaded nanostructured lipid carrier; 4T1, murine breast cancer cell line.
Statistics: Two-way ANOVA followed by Bonferroni's *t*-test (relative tumour volume) and one-way ANOVA followed by Tukey's *t*-test (tumour doubling time), $P < 0.05$
[a] Statistically different from blank-NLC.
[b] Statistically different from free DOX.
[c] Statistically different from NLC-DOX.

tumour growth of breast cancer in humans [43]. This model allows the use of immunocompetent mice, which is an important feature, as the immune system plays an import role in tumour progression [44].

DOX and NLC-DOX showed very low antitumour activity (Table 5) and no statistic differences were seen between them and the negative control (Blank-NLC) regarding tumour growth (Fig. 4A and B). One of the aims of drug combination and synergism studies is dose reduction, in order to produce less to none side effects. Therefore, a spaced DOX dose regimen was used herein (4 mg/kg of DOX, every three days) in order to reduce the well-known side effects of the antineoplastic. This explains the low activity obtained by free DOX and NLC-DOX in our study. Low DOX activity was already found in other works where this dose regimen was used [45,46].

NLC-DOX-SC and free DOX + free SC (in their synergistic molar ratio of DOX:SC 1:1.9) showed better control of the tumour growth when compared to free DOX (Table 5). It is known that NLC can interfere in the tumour microenvironment. To quote some examples, NLC have shown a higher anti-angiogenic effect [47] and enhanced the infiltration of CD3+ and CD8+ cells in the tumour tissue [48] than the correspondent free drugs. Nevertheless, in these examples, NLC presented higher cytotoxicity and higher antitumour activity than the free drugs, which was not seen in our case. This shows that the DOX combination with SC is the responsible for the augmented activity seen for NLC-DOX-SC and not DOX controlled release, as anticancer activity both *in vitro* (Fig. 3B) and *in vivo* (Fig. 4A, B, C and Table 5) were similar between free DOX and NLC-DOX and between free DOX + free SC and NLC-DOX-SC.

This is the first study that has evaluated DOX:SC combination *in vivo*, showing that SC is a potent enhancer of DOX anticancer activity both *in vitro* and *in vivo*. There was an expectation that, *in vivo*, the synergism between DOX and SC might not be observed for the free combination, but only for the NLC-DOX-SC treated animals. Many works that have co-loaded two different molecules in a same nanocarrier have shown that if their pharmacokinetics is different, this will result in lower antitumour activity of the free combination compared to the co-loaded nanocarrier, as the synergic ratio will be maintained, *in vivo*, only for the latter [49–51]. Free DOX + free SC (in their synergistic molar ratio of DOX:SC 1:1.9) and NLC-DOX-SC did not show statistical differences between them regarding antitumour activity (Fig. 4A, B, C and Table 5), indicating that DOX and SC may have arrived together in the tumour despite being administered in their free form.

Interestingly, all the tumours presented extensive necrosis (Fig. 5). Many works have shown that DOX generates necrosis area within the tumour [52,53]. On the contrary, the necrosis seen for Blank-NLC administered animals probably is due to the fact that large tumour volumes were observed for this group by the end of the study (Fig. 4A and C) [54,55].

The results of the study are clear in showing that the combination between DOX and SC in the molar ratio of 1:1.9 (DOX:SC) hugely increases DOX anticancer activity in a triple negative breast cancer model, either in their free form or co-loaded in NLC. Besides maintaining the synergism between DOX and SC, NLC-DOX-SC showed to be a safer option than the free combination (free DOX + free SC) when body weight variation was analysed (Fig. 4D). Blank-NLC administered animals presented weight gain throughout the treatment period, showing that the tumours *per se* did not lead to weight loss. On the other hand, it is possible to see that free DOX + free SC (in their synergistic molar ratio of DOX:SC 1:1.9) generate an expressive weight loss in the animals, indicating their toxicity. DOX systemic administration is related to a reduction in food intake, induction of oral and peptic ulcers and intestinal inflammation, which eventually lead to anorexia and cachexia states, being weight loss an indicator of general health [56–59]. In the meanwhile, animals treated with NLC-DOX-SC maintained a steady weight. Other studies have also reported that NLC can prevent body weight loss in mice caused by DOX [60,61]. Although DOX controlled release did not enhance DOX anticancer activity, it probably diminished its side effects. The maintenance of weight during NLC-DOX-SC treatment is probably linked to the DOX controlled release seen in Fig. 3A, with lower DOX content disposal in the systemic circulation.

Moreover, it is important to emphasise that even though free DOX + free SC caused the same weight loss that free DOX (showing that free SC did not engender weigh loss), free SC did show toxicological effects. Behaviour examination showed that free SC injection caused considerable irritability in the animals. This is probably due to the materials that were used to disperse SC in order to allow its intravenous administration. Although ethanol, polyethylene glycol 400, and Tween™ 80 are FDA approved and very common materials for intravenous administration, their use might cause side effects [62,63]. This shows that SC loading in NLC is a form to mitigate the inconvenience caused by surfactants and solvents that are necessary to disperse hydrophobic molecules like SC.

NLC-DOX-SC also has a less myelosuppressive effect than free DOX + free SC (Table 6). DOX is known as a myelosuppressive drug and targets proliferative cells, including stem cells in bone marrow [1,3]. Encapsulation of chemotherapeutic agents within nanoparticles is a strategy to reduce myelosuppression, as nanoparticles accumulate in a lower extent in the bone marrow [64].

Histopathological analyses have shown that the treatments reduced spleen size and liver inflammation (Fig. 5). It is well reported that 4T1 inoculation leads to splenomegaly and liver inflammation caused by granulocytic infiltrates [65,66]. As DOX can reduce spleen and liver haematopoiesis [67,68], this explains the spleen size reduction and less liver inflammatory infiltrates seen after the treatments.

Finally, cardiac damage was expected as it is DOX's most known side effect [1,3]. Although an increasement in CK values was found for the free DOX group (Table 7), histopathological analysis (Fig. 5) did not find any changes in heart tissue for this group. This apparent contradiction probably is due to the fact that DOX administration regimen was more spaced in our experiments, leading to none to fewer cardiotoxicity.

5. Conclusion

In this work, we have shown that DOX and SC are synergistic or antagonistic depending on their molar ratio and the Fa, in MDA-MB-231 and 4T1 cells. This is the first study that has shown the importance

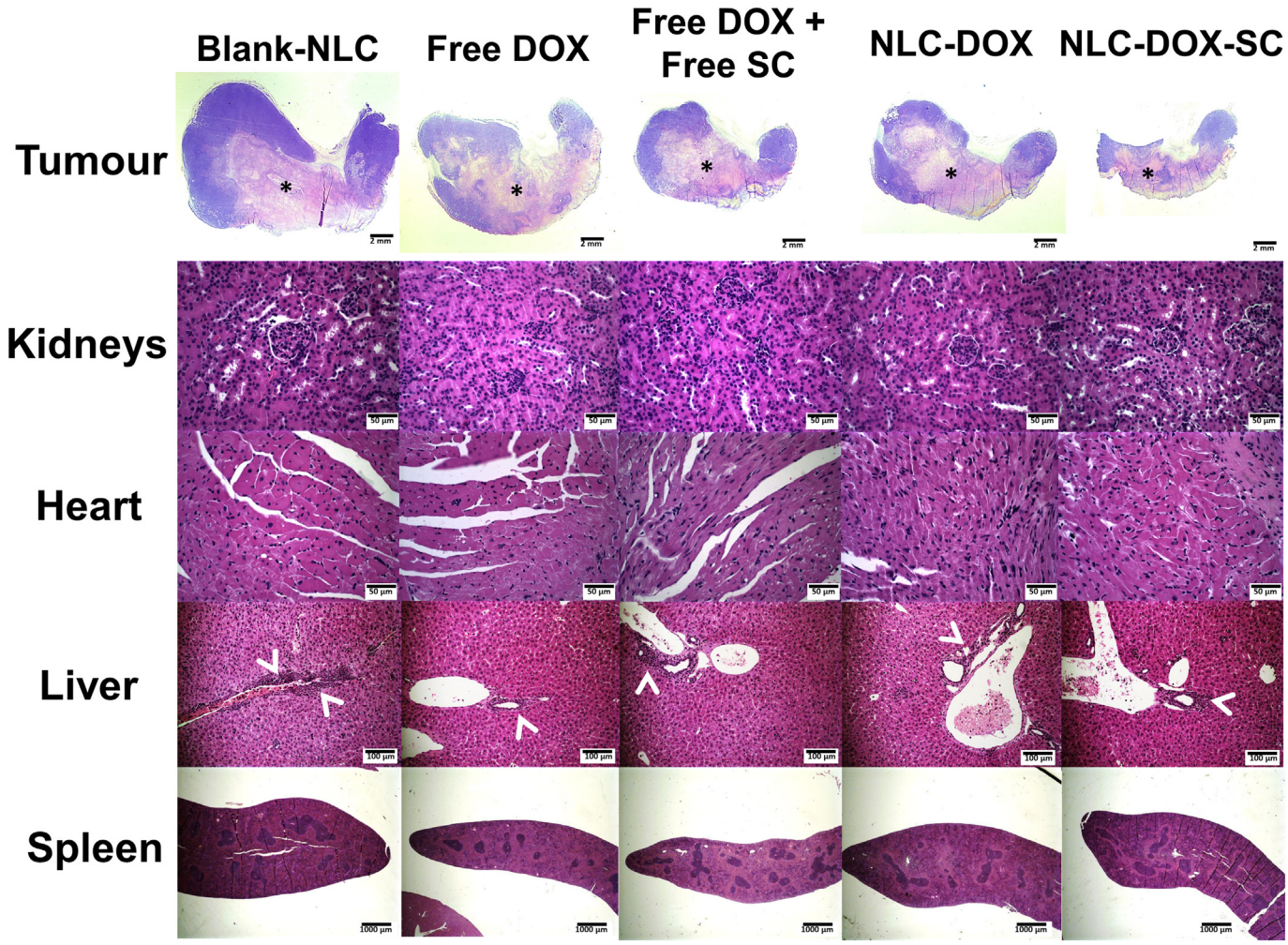

Fig. 5. Histological longitudinal sections (4 μm) stained by haematoxylin and eosin of tumours (0.67× zoom), kidneys (40× zoom), heart (40× zoom), liver (20× zoom), and spleen (2× zoom) from mice after 14 days of treatment. 5-weeks old female mice were inoculated with 4T1 cells subcutaneously and administrations (Blank-NLC, free DOX, free DOX + free SC, NLC-DOX, and NLC-DOX-SC) were started after 8 days of inoculation. Note: Black asterisks represent the necrotic areas in the tumours and white arrows represent the inflammatory infiltrates in the liver.
Abbreviation: 4T1; murine breast cancer cell line; DOX, doxorubicin; SC, sclareol; Blank-NLC, unloaded nanostructured lipid carriers; NLC-DOX, doxorubicin-loaded nanostructured lipid carriers; NLC-DOX-SC, doxorubicin and sclareol in their synergic molar ratio co-loaded nanostructured lipid carrier; free DOX + free SC, doxorubicin and sclareol in their synergic molar ratio; ANOVA, analysis of variance.

Table 6
Haematological results obtained from the blood collected from the animals after 14 days of treatment. Values are expressed as mean ± standard error of the mean, n = 6.

	Reference values [18]	Blank-NLC	Free DOX	Free DOX + Free SC	NLC-DOX	NLC-DOX-SC
WBC ($\times 10^3$/μL)	2.0–10.0	80.8 ± 8.2	31.7 ± 2.3[a]	24.1 ± 2.4[a]	41.1 ± 2.8[a]	34.8 ± 1.6[a]
RBC ($\times 10^6$/μL)	7.0–11.0	6.3 ± 0.1	4.6 ± 0.1[a,b,c]	4.4 ± 0.2[a,b,c]	5.2 ± 0.1[a]	5.0 ± 0.1[a]
HCT (%)	40.0–50.0	31.8 ± 0.4	22.2 ± 0.4[a,b,c]	21.7 ± 0.8[a,b,c]	26.1 ± 0.3[a]	25.5 ± 0.3[a]
HGB (g/dL)	13.0–18.0	12.3 ± 0.3	7.9 ± 0.1[a,b,c]	7.7 ± 0.2[a,b,c]	9.6 ± 0.2[a]	9.0 ± 0.2[a]
RDW (%)	11.0–15.0	14.5 ± 0.3	13.3 ± 0.2[a]	13.6 ± 0.1[a]	14.0 ± 0.1	13.9 ± 0.0
PLT ($\times 10^3$/μL)	1000–2000	320 ± 13	279 ± 8	310 ± 33	333 ± 15	362 ± 29

Abbreviations: WBC, white blood cells; RBC, red blood cells; HCT, haematocrit; HGB, haemoglobin; RDW, red cells distribution width; PLT, platelets; Blank-NLC, unloaded nanostructured lipid carrier; NLC-DOX, doxorubicin loaded nanostructured lipid carrier; NLC-DOX-SC, doxorubicin and sclareol in their synergic molar ratio co-loaded nanostructured lipid carrier.
Statistics: One-way analysis of variance (ANOVA) followed by Tukey's *t*-test, $P < 0.05$.
[a] Statistically different from NLC.
[b] Statistically different from NLC-DOX.
[c] Statistically different from NLC-DOX-SC.

of certain ratios between DOX and SC to evoke the DOX enhancing potential of SC. Moreover, it was shown that it is possible to co-load both molecules in NLC, producing nanocarriers with good physiochemical characteristics and with the capability to control DOX release. This is also the first study that has tested DOX:SC combination *in vivo*, showing that SC not only enhances DOX anticancer activity *in*

Table 7
Biochemical results obtained from the plasma of the animals after 14 days of treatment. Values are expressed as mean ± standard error of the mean, n = 6.

	Blank-NLC	Free DOX	Free DOX + Free SC	NLC-DOX	NLC-DOX-SC
Creatinine (mg/dL)	0.36 ± 0.01	0.35 ± 0.02	0.36 ± 0.01	0.36 ± 0.00	0.30 ± 0.00[a,b,d,e]
Urea (mg/dL)	45.9 ± 1.0	45.5 ± 3.9	46.0 ± 1.0	41.2 ± 2.0	41.0 ± 2.2
AST (U/L)	106.5 ± 2.5	120.5 ± 8.1	96.9 ± 3.6[c,d]	112.5 ± 3.5	123.1 ± 5.8
Ck (U/L)	810 ± 55	996 ± 31[b,c,e]	777 ± 33	661 ± 58	796 ± 44

Abbreviations: AST, aspartate aminotransferase; CK, total creatine kinase; Blank-NLC, unloaded nanostructured lipid carrier; NLC-DOX, doxorubicin loaded nanostructured lipid carrier; NLC-DOX-SC, doxorubicin and sclareol co-loaded nanostructured lipid carrier.
Statistics: One-way analysis of variance (ANOVA) followed by Tukey's *t*-test, $P < 0.05$.
[a] Statistically different from NLC.
[b] Statistically different from NLC-DOX.
[c] Statistically different from NLC-DOX-SC.
[d] Statistically different from free DOX.
[e] Statistically different from free DOX + free SC.

vitro but also *in vivo*. Finally, NLC-DOX-SC shows to be a superior option over the free combination as it maintains the synergism between DOX and SC in triple negative breast cancer models and is less toxic (less myelossupressive, prevents weight loss and behaviour alterations) than the free combination, showing the benefits of nanomedicine in reducing chemotherapy side effects.

Supplementary data to this article can be found online at https://doi.org/10.1016/j.lfs.2019.116678.

Acknowledgments

The authors would like to acknowledge the LNLS Synchrotron (Campinas, Brazil) for the use of SAXS-1 beamline and CAPI (Centre of acquisition and processing of images, UFMG, Belo Horizonte, Brazil) for the use of Cytation™ 5.

Financial and competing interest disclosure

This work was supported by Minas Gerais State Agency for Research and Development (FAPEMIG, Brazil, grant APQ-02489014) and by the Brazilian agencies CAPES (Coordination for the Improvement of Higher Education Personnel, PhD scholarships for G.S.M. Borges, J.O. Silva, and R.S. Fernandes) and CNPq (National Council for Scientific and Technological Development, grant 427798/2018-3). The authors have no other relevant affiliations or financial involvement with any organisation or entity with a financial interest in or financial conflict with the subject matter or materials discussed in the manuscript apart from those disclosed. The authors state that they have no conflicts of interest and have received no payment in preparation of this manuscript. All authors have approved the final article.

References

[1] C. Carvalho, R.X. Santos, S. Cardoso, S. Correia, P.J. Oliveira, M.S. Santos, P.I. Moreira, Doxorubicin: the good, the bad and the ugly effect, Curr. Med. Chem. 16 (2009) 3267–3285.
[2] O. Tacar, P. Sriamornsakb, C.R. Dassa, Doxorubicin: an update on anticancer molecular action, toxicity and novel drug delivery systems, J. Pharm. Pharmacol. 65 (2012) 157–170.
[3] Y. Octavia, C.G. Tocchetti, K.L. Gabrielson, H.J. Crijns, A.L. Moens, Doxorubicin-induced cardiomyophaty: from molecular mechanisms to therapeutic strategies, J. Mol. Cell. Cardiol. 52 (6) (2012) 1213–1225.
[4] T.C. Chou, Theoretical basis, experimental design and computerized simulation of synergism and antagonism in drug combination studies, Pharmacol. Rev. 58 (3) (2006) 621–681.
[5] K. Dimas, D. Kokkinopulos, C. Demetzos, B. Vaos, M. Marselos, M. Malamas, T. Tzavaras, The effect of sclareol on growth and cell cycle progression of human leukemic cell lines, Leuk. Res. 23 (3) (1999) 217–234.
[6] K. Dimas, C. Demetzos, B. Vaos, P. Ionnidis, T. Trangas, Labdene type diterpenes down-regulate the expression of *c-myc* protein, but not of *bcl-2* in human leukemia T-cells undergoing apoptosis, Leuk. Res. 25 (6) (2001) 449–454.
[7] K. Dimas, S. Hatziantoniou, S. Tseleni, H. Khan, A. Georgopoulos, K. Alevizopoulos, J.H. Wyche, P. Pantazis, C. Demetzos, Sclareol induces apoptosis in human HCT116 colon cancer cells *in vitro* and suppression of HCT116 tumor growth in immunodeficient mice, Apoptosis 12 (4) (2007) 685–694.
[8] S. Hatziantoniou, K. Dimas, A. Georgopoulos, N. Sotiriadou, C. Demetzos, Cytotoxic and antitumor activity of liposome-incorporated sclareol against cancer cell lines and human colon cancer xenografts, Pharmacol. Res. 53 (1) (2006) 80–87.
[9] L.G. Mahaira, C. Tsimplouli, N. Sakellaridis, K. Alevizopoulos, C. Demetzos, Z. Han, P. Pantazis, K. Dimas, The labdane diterpene sclareol (labd-14-ene-8,13-diol) induces apoptosis in human tumor cell lines and supression of tumor growth *in vivo* via a p53-independent mechanism of action, Eur. J. Pharmacol. 666 (2011) 173–182.
[10] A. Paradissis, S. Hatziantoniou, A. Georgopoulos, A.G. Psarra, K. Dimas, C. Demetzos, Liposomes modify the subcellular distribution of sclareol uptake by HCT-116 cancer cell lines, Biomed. Pharmacother. 61 (2007) 120–124.
[11] A. Paradissis, S. Hatziantoniou, A. Georgopoulos, K. Dimas, C. Demetzos, Uptake studies of free and liposomal sclareol by MCF-7 and H-460 human cancer cell lines, in: M.R. Mozafari (Ed.), Nanomaterials and Nanosystems for Biomedical Applications, Springer, Dordretch, 2007, pp. 125–133.
[12] K. Dimas, M. Papadaki, C. Tsimplouli, S. Hatziantoniou, K. Alevizopoulos, P. Pantazis, C. Demetzos, Labd-14-ene-8,13-diol (sclareol) induces cell cycle arrest and apoptosis in human breast cancer and enhances the activity of anticancer drugs, Biomed. Pharmacother. 60 (3) (2006) 127–133.
[13] F. Perche, V.P. Torchilin, Cancer cell spheroids as a model to evaluate chemotherapy protocols, Cancer Biol. Ther. 13 (12) (2012) 1205–1213.
[14] M.S. Franco, M.C. Oliveira, Ratiometric drug delivery using non-liposomal nanocarriers as an approach to increase efficacy and safety of combination chemotherapy, Biomed. Pharmacother. 96 (2017) 584–595.
[15] A. Beloqui, M.A. Solinís, A. Rodríguez-Gascón, A.J. Almeida, V. Préat, Nanostructured lipid carriers: promising drug delivery systems for future clinics, Nanomedicine 12 (2016) 143–161.
[16] S.V. Mussi, R.C. Silva, M.C. Oliveira, C.M. Lucci, R.B. Azevedo, L.A.M. Ferreira, New approach to improve encapsulation and antitumor activity of doxorubicin loaded in solid lipid nanoparticles, Eur. J. Pharm. Sci. 48 (1–2) (2013) 282–290.
[17] M.S. Oliveira, S.V. Mussi, D.A. Gomes, M.I. Yoshida, F. Frezard, V.M. Carregal, L.A.M. Ferreira, α-Tocopherol succinate improves encapsulation and anticancer activity of doxorubicin loaded in solid lipid nanoparticles, Colloids Surf. B: Biointerfaces 140 (2016) 246–253.
[18] N. Everds, Hematology of the mouse, in: H.J. Hedrich, G. Bullock (Eds.), The Laboratory Mouse, first ed., Academic Press, San Diego, 2004, pp. 271–286.
[19] C. Denkert, C. Liedtke, A. Tutt, G. von Minckwitz, Molecular alterations in triple-negative breast cancer—the road to new treatment strategies, Lancet 389 (2017) 2430–2442.
[20] S. Cleator, W. Heller, R.C. Coombes, Triple-negative breast cancer: therapeutic options, Lancet Oncol. 8 (2007) 235–244.
[21] R. Santanda-Davila, E.A. Perez, Treatment options for patients with triple-negative breast cancer, J. Hematol. Oncol. 3 (42) (2010).
[22] A. Roy, M. Ahir, S. Bhattacharya, P.K. Parida, A. Adhikary, K. Jana, M. Ray, Induction of mitochondrial apoptotic pathway in triple negative breast carcinoma cells by methylglyoxal via generation of reactive oxygen species, Mol. Carcinog. 56 (9) (2017) 2086–2103.
[23] X. Zhao, Q. Chen, W. Liu, Y. Li, H. Tang, X. Liu, X. Yang, Codelivery of doxorubicin and curcumin with lipid nanoparticles results in improved efficacy of chemotherapy in liver cancer, Int. J. Nanomedicine 10 (2014) 257–270.
[24] S.V. Mussi, R. Sawant, F. Perche, M.C. Oliveira, R.B. Azevedo, L.A. Ferreira, V.P. Torchilin, Novel nanostructured lipid carrier co-loaded with doxorubicin and docosahexaenoic acid demonstrates enhanced *in vitro* and overcomes drug resistance in MCF-7/Adr cells, Pharm. Res. 31 (2014) 1882–1892.
[25] S.V. Mussi, G. Parekh, P. Pattekari, T. Levchenko, Y. Lvovo, L.A.M. Ferreira, V.P. Torchilin, Improved pharmacokinetics and enhanced tumor growth inhibition using a nanostructured lipid carrier loaded with doxorubicin and modified with a layer-by-layer polyelectrolyte coating, Int. J. Pharm. 495 (2015) 186–193.
[26] M.S. Oliveira, B. Aryasomayajula, B. Pattni, S.V. Mussi, L.A.M. Ferreira, V.P. Torchilin, Solid lipid nanoparticles co-loaded with doxorubicin and α-tocopherol succinate are effective against drug-resistant cancer cells in monolayer and 3-D spheroid cancer cell models, Int. J. Pharm. 512 (2016) 292–300.
[27] G. Rai, S. Mishraa, S. Sumana, Y. Shuklaa, Resveratrol improves the anticancer

effects of doxorubicin in vitro and in vivo models: a mechanistic insight, Phytomedicine 23 (2016) 233–242.
[28] J.O. Silva, S.E.M. Miranda, E.A. Leite, A.P. Sabino, K.B.G. Borges, V.N. Cardoso, G.D. Cassali, A.G. Guimarães, M.C. Oliveira, A.L.B. Barros, Toxicological study of a new doxorubicin-loaded pH sensitive liposome: a preclinical approach, Toxicol. Appl. Pharmacol. 352 (2018) 162–169.
[29] C. Núñez, J.L. Capelo, G. Igrejas, A. Alfonso, L.M. Botana, C. Lodeiro, An overview of the effective combination therapies for the treatment of breast cancer, Biomaterials 97 (2016) 34–50.
[30] J.A. Kempa, M.S. Shim, C.Y. Heo, Y.J. Kwon, "Combo" nanomedicine: co-delivery of multi-modal therapeutics for efficient, targeted, and safe cancer therapy, Adv. Drug Deliv. Rev. 98 (2016) 3–18.
[31] M.R. King, Z.J. Mohamed, Dual nanoparticle drug delivery: the future of anticancer therapies? Nanomedicine 12 (2) (2017) 95–98.
[32] S.Z. Vahed, R. Salehia, S. Davarana, S. Sharifi, Liposome-based drug co-delivey systems in cancer cells, Mater. Sci. Eng. C Mater. Biol. Appl. 71 (2017) 1327–1341.
[33] E.C. Chen, A.T. Fathi, A.M. Brunner, Reformulating acute myeloid leukemia: liposomal cytarabine and daunorubicin (CPX-351) as an emrging therapy for secondary AML, Onco. Targets. Ther. 11 (2018) 3425–3434.
[34] S. Taurin, H. Nehoff, K. Greish, Anticancer nanomedicine and tumor vascular permeability: where is the missing link? J. Control. Release 164 (2012) 265–275.
[35] R.S. Fernandes, J.O. Silva, L.O. Monteiro, E.A. Leite, G.D. Cassali, D. Rubello, V.N. Cardoso, L.A. Ferreira, M.C. Oliveira, A.L. de Barros, Doxorubicin-loaded nanocarriers: a comparative study of liposome and nanostructured lipid carrier as alternatives for cancer therapy, Biomed. Pharmacother. 85 (2016) 252–257.
[36] M.S. Oliveira, G.C. Goulart, L.A. Ferreira, G. Carneiro, Hydrophobic ion pairing as a strategy to improve drug encapsulation into lipid nanocarriers for the cancer treatment, Expert Opin. Drug Deliv. 14 (2017) 983–995.
[37] Z. Shao, J. Shao, B. Tan, S. Guan, Z. Liu, Z. Zhao, F. He, J. Zhao, Targeted lung cancer therapy: preparation and optimization of transferrin-decorated nanostructured lipid carriers as novel nanomedicine for co-delivery of anticancer drugs and DNA, Int. J. Nanomedicine 10 (2015) 1223–1233.
[38] G.A. Castro, A.L.L.R. Coelho, G.A. Mahecha, R.L. Oréfice, L.A. Ferreira, Formation of ion pairing to improve encapsulation and stability and to reduce skin irritation of retinoic acid loaded in solid lipid nanoparticles, Int. J. Pharm. 381 (2009) 77–83.
[39] W. Lv, S. Zhao, H. Yu, N. Li, V.M. Garamus, Y. Chen, P. Yin, R. Zhang, Y. Gong, A. Zou, Bruceajavanic oil-loaded nanostructured lipid carriers (BJO NLCs): preparation, characterization and in vitro evaluation, Colloids Surf. A Physicochem. Eng. Asp. 504 (2016) 312–319.
[40] G. Lukowski, J. Kasbohm, P. Pflegel, A. Lling, H. Wulff, Crytallographic investigation of cetylpalmitate solid lipid nanoparticles, Int. J. Pharm. 196 (2000) 201–205.
[41] H.S. Rahman, A. Rasedee, A.B. Abdul, N.A. Zeenathul, H.H. Othman, S.K. Yeap, C.W. How, W.A. Hafiza, Zerumbone-loaded nanostructured lipid carrier induces G2/M cell cycle arrest and apoptosis via mitochondrial pathway in a human lymphoblastic leukemia cell line, Int. J. Nanomedicine 9 (2014) 527–538.
[42] S. Selvamuthkumar, R. Velmuruga, Nanostructured lipid carriers: a potential drug carrier for cancer chemotherapy, Lipids Health Dis. 11 (159) (2012) 1–8.
[43] P. Kaur, G.M. Nagaraja, H. Zheng, D. Gizachew, M. Galukande, S. Krishnan, A. Asea, A mouse model for triple-negative breast cancer tumor-initiating cells (TNBC-TICs) exhibits similar aggressive phenotype to the human disease, BMC Cancer 12 (120) (2012).
[44] O.J. Finn, Immuno-oncology: understanding the function and dysfunction of the immune system in cancer, Ann. Oncol. 23 (2012) viii6–9.
[45] C. Polydorou, F. Mpekris, P. Papageorgis, C. Voutouri, T. Stylianopoulos, Pirfenidone normalizes the tumor microenvironment to improve chemotherapy, Oncotarget 8 (15) (2017) 24506–24517.
[46] G. Venkatraman, M.G.K. Benesch, X. Tang, J. Dewald, T.P.W. McMullen, D.N. Brindley, Lysophosphatidate signalling stabilizes Nrf2 and increases the expression of genes involved in drug resistance and oxidative stress responses: implications for cancer treatment, FASEB J. 29 (3) (2014) 772–785.
[47] N. Nordin, S.K. Yeap, C. Tsimplouli, H.S. Rahman, N.R. Zamberi, N. Abu, N.E. Mohamad, C.W. How, M.J. Masarudin, R. Abdullah, N.B. Alitheen, *In vitro* cytotoxicity and anticancer effects of citral nanostructured lipid carrier on MDA-MB-231 human breast cancer cell, Sci. Rep. 9 (1) (2019) 1614.
[48] C. Deng, M. Jia, G. Wei, T. Tan, Y. Fu, H. Gao, X. Sun, Q. Zhang, T. Gong, Z. Zhang, Inducing optimal antitumor immune response through coadministering iRGD with pirarubicin loaded nanostructured lipid carriers for breast cancer therapy, Mol. Pharm. 14 (2017) 296–309.
[49] D. Zucker, Y. Barenholz, Optimization of vincristine–topotecan combination – paving the way for improved chemotherapy regimens by nanoliposomes, J. Control. Release 146 (2010) 326–333.
[50] M.Y. Wong, G.N. Chiu, Liposome formulation of co-encapsulated vincristine and quercetin enhanced antitumor activity in a trastuzumab-intensive breast tumor xenograft model, Nanomedicine 7 (6) (2011) 834–840.
[51] Y. Liu, J. Fang, Y.J. Kim, M.K. Wong, P. Wang, Codelivery of doxorubicin and paclitaxel by cross-linked multilamellar liposome enables synergistic antitumor activity, Mol. Pharm. 11 (5) (2014) 1651–1661.
[52] G. Li, Y. Liang, C. Sun, X. Peng, N. Hao, M. Liu, W. Gao, H. Wu, B. He, Effective combination therapy of percutaneous ethanol injection and chemotherapy based on injectable low molecular weight gels, Artif. Cells Nanomed. Biotechnol. 46 (2) (2018) 683–693.
[53] A.M. Butt, M.C.I.M. Amin, H. Katas, N.A.A. Murad, R. Jamal, P. Kesharwani, Doxorubicin and siRNA codelivery of chitosan-coated pH-responsive mixed micellar polyplexes for enhanced cancer therapy in multidrug-resistant tumors, Mol. Pharm. 13 (2016) 4179–4190.
[54] M. Zhu, L. Jiang, M.L. Fabiilli, A. Zhang, J.B. Fowlkes, L.X. Xu, Treatment of murine tumors acoustic droplet vaporization-enhanced high intensity focused ultrasound, Phys. Med. Biol. 58 (2013) 6179–6191.
[55] K. Tao, M. Fang, J. Alroy, G.G. Sahagian, Imagable 4T1 model for the study of late stage breast cancer, BMC Cancer 8 (228) (2008).
[56] L. Wang, Q. Chen, H. Qi, C. Wang, C. Wang, J. Zhang, L. Dong, Doxorubicin-induced systemic inflammation is driven by upregulation of toll-like receptor TLR4 and endotoxin leakage, Cancer Res. 76 (22) (2016) 6631–6642.
[57] L.A. Gilliam, L.F. Ferreira, J.D. Bruton, J.S. Moylan, H. Westerblad, D.K. St Clair, M.B. Reid, Doxorubicin acts through tumor necrosis factor receptor subtype 1 to cause dysfunction of murine skeletal muscle, J. Appl. Physiol. 107 (6) (2009) 1935–1942.
[58] V.Z. Agrba, D.D. Karal-Ogly, T.E. Gvozdik, P.A. Kaplanyan, N.P. Demenkova, I.A. Gvaramiya, E.I. Mukhametzyanova, O.A. Shamsutdinova, Y.P. Chugev, S.S. Kalsina, A.G. Konoplyannikov, D.E. Araviashvili, I.N. Klots, B.A. Lapin, Use of mesenchymal stem cells for possible repair of doxorubicin-damaged organs and tissues in experimental monkeys, Bull. Exp. Biol. Med. 165 (1) (2018) 101–104.
[59] J.A. Zombeck, E.G. Fey, G.G. Lyng, S.T. Sonis, A clinically translatable mouse model for chemotherapy-related fatigue, Comp. Med. 63 (6) (2013) 491–497.
[60] X. Dong, W. Wang, H. Qu, D. Han, J. Zheng, G. Sun, Targeted delivery of doxorubicin and vincristine to lymph cancer: evaluation of novel nanostructured lipid carriers *in vitro* and *in vivo*, Drug Deliv. 23 (4) (2016) 1374–1378.
[61] S. Ni, L. Qiu, G. Zhang, H. Zhou, Y. Han, Lymph cancer chemotherapy: delivery of doxorubicin-gemcitabine prodrug and cincristine by nanostructured lipid carriers, Int. J. Nanomedicine 12 (2017) 1565–1576.
[62] E.A. Thackaberry, X. Wang, M. Schweiger, K. Messick, N. Valle, B. Dean, A. Sambrone, T. Bowman, M. Xie, Solvent-based formulations for intravenous mouse pharmacokinetics studies: tolerability and recommended solvent dose limits, Xenobiotica 44 (3) (2014) 235–241.
[63] A.G. Ellis, N.A. Crinis, L.K. Webster, Inhibition of etoposide elimination in the isolated perfused rat liver by Cremophor EL and Tween 80, Cancer Chemother. Pharmacol. 38 (1996) 81–87.
[64] J. Zhou, X. Zhang, M. Li, W. Wu, X. Sun, L. Zhang, T. Gong, Novel lipid hybrid albumin nanoparticle greatly lowered toxicity of piraubicin, Mol. Pharm. 10 (10) (2013) 3832–3841.
[65] S.A. duPré, K.W. Hunter Jr., Murine mammary carcinoma 4T1 induces a leukemoid reaction with splenomegaly: association with tumor-derived growth factors, Exp. Mol. Pathol.. 82(1) (2007) 12–24.
[66] S. Tabariès, V. Ouellet, B.E. Hsu, M.G. Annis, A.A.N. Rose, L. Meunier, E. Carmona, C.E. Tam, A. Mes-Masson, P.M. Siegel, Granulocytic immune infiltrates are essential for the efficient formation of breast cancer liver metastases, Breast Cancer Res. 17 (45) (2015).
[67] C.R. Comereski, W.M. Peden, T.J. Davidson, G.L. Warner, R.S. Hirth, J.D. Frantz, BR96-doxorubicin conjugate (BMS-182248) versus doxorubicin: a comparative toxicity assessment in rats, Toxicol. Pathol. 22 (5) (1994) 473–488.
[68] A.C. Gregório, N.A. Fonseca, V. Moura, M. Lacerda, P. Figueiredo, S. Simões, S. Dias, J.N. Moreira, Inoculated cell density as a determinant factor of the growth dynamics and metastatic efficiency of a breast cancer murine model, PLoS One 11 (11) (2016) e0165817.